IEEE Access
Multidisciplinary ⋮ Rapid Review ⋮ Open Access Journal

Received January 12, 2022, accepted February 10, 2022, date of publication February 21, 2022, date of current version March 2, 2022.

Digital Object Identifier 10.1109/ACCESS.2022.3153127

Pre-Landing Control for a Legged Robot Based on Tiptoe Proximity Sensor Feedback

RYUKI SATO[1], (Member, IEEE), HIKARU ARITA[2], (Member, IEEE), AND AIGUO MING[3], (Member, IEEE)

[1]Department of Aerospace Engineering, Nagoya University, Nagoya, Aichi 464-8603, Japan
[2]Department of Robotics, College of Science and Engineering, Ritsumeikan University, Kusatsu, Shiga 525-8577, Japan
[3]Department of Mechanical Engineering and Intelligent Systems, The University of Electro-Communications, Chofu, Tokyo 182-8585, Japan

Corresponding author: Ryuki Sato (ryuki.sato@mae.nagoya-u.ac.jp)

This work was supported by JSPS KAKENHI Grant Number JP20K22389.

ABSTRACT The moment a legged robot touches the ground, the tip of its toe can experience a significant impact force. It is preferable to keep the landing impact force small because it causes imbalance and damage to the frame, motors, gears, and other components of the robot legs. In this paper, we propose a control method to mitigate the landing impact force by preliminary motion based on the proximity information of the tiptoe before landing. A proximity sensor is mounted on the tiptoe to detect the ground before landing, and feedback control is applied according to the sensor output to reduce the impact force. In landing experiments using a one-legged robot equipped with a proximity sensor on a tiptoe, we evaluated the effects of changing the sensor offset distance and the feedback gains on impact force mitigation. The results show that the landing impact force was mitigated by reducing the relative velocity of the tiptoe and the ground using the proposed proximity feedback control.

INDEX TERMS Legged robot, proximity sensor, landing control, ground contact, impact mitigation.

I. INTRODUCTION

A legged robot alternates between touching the ground and taking off on the tips of its toes while walking or running. Since this movement method allows the robot to select and move any discrete grounding points, the robot is expected to exhibit high movement performance, especially on rough terrain. Many research groups and companies have been developing legged robots for use at disaster sites and in human environments [1]–[4].

Due to the characteristics of legged locomotion mentioned above, the landing impact force is applied to every step on tiptoes that collide with the ground during travel. The more agile the movement (such as running, where the relative speed of the collision between the tiptoe and the ground becomes high), the more significant the impact force applied to the robot. Because recent research on legged robots has focused not only on quasi-static walking but also agile locomotion such as running and jumping, aiming to improve travel speed and mobility, it is necessary to manage the landing impact.

The associate editor coordinating the review of this manuscript and approving it for publication was Zheng H. Zhu.

Large impact forces can cause damage to the robot's frame, transmission mechanism, and joint actuators. In particular, the small teeth of gears, commonly used as a reducer for legged robots, are very fragile and easily broken by the impact force. In addition, energy dissipation due to rigid body collision between the tiptoe and the ground may waste the limited electric energy of the robot [5]. The slight bounce of the tiptoe due to the landing impact force causes slippage as the friction force between the tiptoe and the ground decreases [6], [7]. For these reasons, mitigating the impact force upon landing is essential for the safe operation of legged robots.

Legged robots can land adaptively using passive or active compliance in the legs. Physical springs and dampers in the robot legs can provide compliance in the legs [8]. Most of these components were inspired by the viscoelasticity around muscle tissues in living animals [9]–[11]. There is also an effort to design nonlinear springs and dampers on the tiptoe mechanism to mitigate the landing impact [5]. Physical springs and dampers in the leg allow robots to passively adapt to momentary landing impacts without being affected by the responsiveness of control computers or active actuators. However, since these physical compliances affect various

motions other than landing (such as walking, running, and jumping), a stiffness design specialized for landing is not always favorable for the motion performance of the legged robot.

Impedance control is a well-known active control method for adaptive gait [12]–[14]. Robot legs are actively controlled to have the desired viscoelasticity according to the load and desired movement. A cooperative control method for human-robot interaction using both visual and force sensors has also been proposed [15]. However, the use of force sensors increases the total cost and weight of the robot. In addition, the force sensor is vulnerable to impact due to its measurement principle, and a large landing impact force in dynamic motion causes sensor failure. Furthermore, a quick response speed is required for sensors and actuators to respond to momentary landing impacts. A series elastic actuator [3], [16], [17] enables reasonable torque control without a force sensor; however, the control bandwidth is limited.

Using a quasi-direct drive actuator that combines a large-capacity motor and a reducer with an extremely low-reduction ratio allows for reasonable force control without a special sensor because the effects of rotor inertia and gear friction can be reduced [18]. In addition, the reflection inertia is reduced by adopting a low-reduction ratio reducer, and the landing impact can be mitigated. Many recent dynamic-legged robots have adopted this actuator configuration, and soft landings have been achieved with proprioceptive force control [2], [19]–[21].

The impact mitigation methods introduced above become actively or passively effective after landing according to the impact of the tiptoe touching down. It is difficult to reduce the impact force immediately after touchdown. To eliminate its effect on the legged robot, an impact mitigation method that is effective from the moment of landing is required. One approach to achieving impact mitigation at touchdown is introducing a pre-landing control before ground contact to control the transition from non-contact to contact.

To achieve pre-landing control, we introduced a proximity sensor to the tiptoe of the robot leg to accurately detect and control the transition from just before to after ground contact. Then, we proposed a pre-landing control based on the proximity information from the tiptoe sensor to mitigate the impact force at landing. In this paper, an optical reflection-type sensor capable of one-dimensional proximity sensing is attached to the tiptoe of a one-legged robot as the first step of introducing a proximity sensor to the tiptoe of the robot. We focus on the non-monotonicity of the sensor output and utilize its unique characteristics to the pre-landing feedback control to mitigate the significant impact force. In the experiments, we observed the landing impact force and behavior of the vertically falling robot in which the proposed pre-landing control was applied. The proposed control method for landing impact mitigation was verified with experimental results with different control parameter values.

The main contribution of this paper is to experimentally show that the problems which cannot be managed by conventional landing impact mitigation methods can be solved by introducing pre-landing control, which is effective before ground contact. In other words, we demonstrated that the impact force applied at the moment of touchdown could be mitigated by the proposed control method using tiptoe optical proximity sensor feedback. The mitigation of the landing impacts is an important issue for realizing dynamic locomotion in a legged robot. With our approach, a proximity sensor that can directly detect the relative relationship with the ground is introduced at the tiptoe to prepare for landing quickly and reflexively only with local information, and therefore it is possible to respond in agile movements of the robot. The proposed method could be easily introduced into other position-controlled legged robots in the future.

The rest of this paper is organized as follows. Section II introduces related works and compares their contributions to our work. Section III presents the proposed pre-landing control method based on proximity information on tiptoe for legged robot landing impact mitigation. Section IV introduces a one-legged robot with a proximity sensor installed on the tiptoe and is used for the landing experiment described in Section V. Section VI presents the results and discussions of landing experiments. The conclusions and future work are provided in Section VII.

II. RELATED WORK

In this section, we introduce related works about pre-landing control for a legged robot to mitigate landing impact and the use of proximity sensors for robot control. Then, we explain the advantages of our approach to solve the problem of legged robot landing.

A. PRE-LANDING CONTROL

The tiptoe trajectory of the swing leg, which was pre-designed so that the relative velocity between the tiptoe and the ground becomes zero at the moment of ground contact to mitigate the landing impact force, was used for several position-controlled legged robots [22], [23].

To pre-design tiptoe trajectory as in these studies, the terminal coordinates of the trajectory, i.e., the contact position of the tiptoe with the environment, should be planned in advance. In other words, ground surface information is required to place tiptoes in an arbitrary position on uneven or deformable terrain. Vision sensors, one of which is usually mounted on the head or torso of the robot, are often used to detect the ground surface on the walking robot path. The relative distance and velocity between the ground and the robot's coordinate system are estimated based on the ground surface information detected by the vision sensor and the robot state measured by internal sensors such as an inertial measurement unit (IMU) and joint encoders. However, the use of visual sensors can lead to occlusion of the ground surface by parts of the robot itself. Modeling and state measurement errors can cause significant landing impact forces

when using pre-designed orbits that require rigor in contact position and contact time. In addition, image processing is generally time-consuming, resulting in a long update cycle, which makes it difficult to apply to dynamic motion.

Several landing impact mitigation controls have been proposed that are robust to terrain information errors and errors in the robot's own state estimation. In [24], landing control for the landing phase of vertical jumping was proposed, in which both landing impact mitigation immediately at the moment of ground contact and posture recovery after landing were considered. To reduce the landing impact, the tiptoe velocity is controlled before landing in the air so that the relative velocity between the feet and the ground is close to 0 m/s at touchdown. The touchdown time and velocity of the robot's center of gravity (CoG) at the ground contact are estimated based on the CoG velocity at the take-off of the jumping motion, which may contain some errors. Nevertheless, even with some estimation error, it was possible to land without excessive impact force due to the pre-landing control. After landing, the robot was able to converge to an equilibrium posture quickly by switching to motion control, which reduced the ground reaction force (GRF).

In [25], a framework for switching between swing leg control and support leg control was proposed to absorb the landing impact. By applying compliance adjustment based on fuzzy control to the swing leg that follows the trajectory planned by the preview control, a large landing impact force was avoided even with errors in the landing time or ground contact position. A humanoid walking on uneven terrain using this control strategy was demonstrated in simulation.

These methods can be expected to be robust to some degree of state estimation error at landing. However, there is a limitation in the applicability of indirect estimation of the tiptoe-to-ground relative relation based on the pre-detected information, and this cannot be used for more dynamic motions. The method that requires control switching in the swing and stance phases is undesirable where an unexpected instantaneous collision can be expected.

B. ROBOT CONTROL USING PROXIMITY SENSOR FEEDBACK

Proximity sensors can detect objects within several hundred millimeters from the sensor surface. Since most proximity sensors are designed to be small and lightweight, they can be mounted in narrow spaces or on uneven surfaces such as the fingertips and the arm surface of the robot [26]. In the same way, proximity sensors can be easily attached to tiptoes in direct contact with the ground. In other words, no occlusion can occur because there can be no obstruction between the sensor and the ground; additionally, estimation error due to modeling errors could not occur. Because the response time of this type of sensor is much shorter than that of a vision sensor, the response delay can be less of a problem even when fast sampling is required for dynamic motion control. In addition, because the sensor can detect the ground without non-contacting it, there is no risk of breaking the tiptoe-attached sensor by the landing impact force.

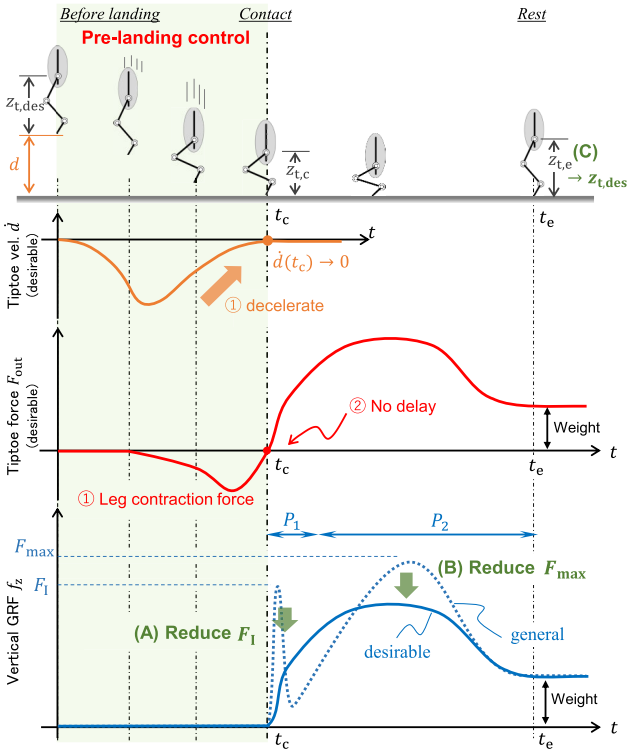

FIGURE 1. Desirable landing performance of legged robot.

For example, in robot control based on proximity perception information, avoidance of collisions with objects and humans [27], [28] and robotic grasp control strategies for accurate object grasping [29], [30] have been studied.

In [31], a control method for a non-contact-to-contact transition of a robot arm utilizing proximity sensor output as a virtual force was proposed. By controlling the emission energy of the optical reflective sensor, the virtual force is adjusted so that the robot arm makes contact with the object using the desired contact force. Experiments using a one-degree-of-freedom robot arm demonstrated that the robot could smoothly transition between non-contact and contact without switching the control strategy.

On the other hand, few studies have introduced proximity sensors to the tiptoe of legged robots. Reference [32] is one of the few examples in which proximity sensors were installed on the soles of a humanoid robot; however, foot proximity information was only used to detect the landing state. To the best of our knowledge, there is no example of landing impact force mitigation using a proximity sensor on the tiptoe of a legged robot aiming to achieve dynamic motion.

C. OUR PROPOSED METHOD

In our proposed method, the landing impact force is mitigated by introducing a pre-landing motion based on proximity information to the active compliance-controlled swing leg from the non-contact state before landing. Since the

proximity sensor can directly and quickly detect the local environment-foot relative state without contact, it is effective even for more dynamic motions than in previous works. For pre-landing control, the virtual reaction force based on the proximity sensor output used in [31] can be introduced into robot control in an integrated manner with compliance control. The seamless control framework from non-ground-contact to ground-contact does not require strict landing timing and precise landing positions and can cope with unexpected collisions in more dynamic-legged locomotion.

III. PRE-LANDING CONTROL FOR LANDING IMPACT MITIGATION

The goal of this study is to achieve a desirable landing by mitigating the impact force immediately after landing due to the pre-movement of the landing, as shown in Fig. 1. In this section, we first consider the ideal landing motion of the robot to mitigate the impact force. Then, we outline a method for realizing the ideal landing motion by using a proximity sensor on a tiptoe. After that, the proposed pre-landing motion control is explained by using the equations of motion of the robot.

A. DESIRABLE LANDING PERFORMANCE

We focus on a series of free-fall motions of a legged robot from the air. As described in [24], it is desirable for the landing motion to mitigate the impact force at the time of landing and then quickly converge to an equilibrium posture. To illustrate the points of interest of the landing motion, we divide the series of free-fall-landing motions into two phases based on the characteristics of the typical landing GRF profile [6] shown in the lower part of Fig. 1: the phase in which the impact force occurs immediately after landing (P_1) and the phase in which the robot is stationary in the equilibrium posture after landing (P_2).

The impact force F_I immediately after landing in P_1 depends on the velocity between the colliding objects. To reduce F_I, the relative velocity between the tiptoe and the ground, $\dot{d}$, should be close to zero just before landing, as shown in the upper graph of Fig. 1. This can be achieved by contracting the leg length z_t relative to the free-falling torso. A negative tiptoe force F_{out} before the tiptoe collides with the ground, as shown in the middle graph of Fig. 1, will bring $\dot{d}$ closer to 0 m/s, thus reducing the impact force, where F_{out} is defined as positive in the direction of the leg extension.

The GRF in P_2 mainly slows down the falling motion of the torso and makes the robot stand still. Even if the impact force F_I can be reduced in P_1, the maximum GRF F_{max} in P_2 should not be excessive because it causes an increase in the load on the actuators and frames and excessive posture fluctuations. To effectively decelerate the falling motion of the torso and prevent excessive GRF after landing, it is desired that F_{out} should be equal to or greater than 0 at ground contact.

If the landing controller is independent of the robot's motion control (e.g., trajectory-following position control), then it is necessary to switch the control scheme before and after landing, leading to an increase in control cost. If the landing control can be integrated into the main motion controller, then the increase in the control cost can be avoided.

In the free-falling motion dealt with in this paper, joint position control at a constant target angle was applied during the entire motion. In other words, in this case of the problem setting, the landing control requirement after touchdown is to reduce the error $\Delta z_{t,e} = z_{t,e} - z_{t,des}$, where $z_{t,e}$ is the actual leg length when the robot comes to rest in the equilibrium posture (hereafter called the ''equilibrium posture''), and $z_{t,des}$ is the desired leg length.

We summarize the requirement for landing control for the ideal landing motion of the legged robot targeted in this paper as follows:

(A) Reduction of the impact force (F_I) at touchdown.
(B) Reduction the maximum GRF (F_{max}) after landing.
(C) Reduction of posture deviation after landing ($|\Delta z_{t,e}|$).

B. PROXIMITY SENSOR FOR PRE-LANDING CONTROL

To detect the relative relationship between the tiptoe and the ground prior to landing, it is desirable to have a sensor that is small enough to be attached directly to the tiptoe, has high accuracy, and has a high sampling rate. Visual sensors such as cameras and LiDAR have problems with occlusion, high measurement error, and low sample rate. A proximity sensor is promising as one of the sensors that can solve these problems.

An optical reflective proximity sensor is generally compact and easy to mount on the tiptoe. This type of sensor consists of a light-emitting element and a light-receiving element that are generally placed next to each other so that their optical axes are parallel. Here, we assume that the object surface (the ground in the case of legged robots) is large enough for the sensor and that the reflectance rate is uniform and constant. The tiptoe-attached optical reflective sensor can detect the approach of the tiptoe and the ground under non-contact condition. The sensor output $s \in [0\ 1]$ varies nonlinearly with the distance between the sensing surface and the object surface ($d + d_o$), as illustrated in the bottom graphs in Fig. 2, where d is the distance from the ground to the tiptoe contact point and d_o is the offset distance from the sensor surface to the tiptoe contact point. The sensor output increases as the tiptoe approaches to the ground and becomes extremely small in the closest approach. Namely, the sensor output, which is photocurrent, become larger the closer the distance between the object and the sensing surface is. The maximum output is obtained when the distance is equal to the focal length. The output suddenly decreases when the distance is shorter than the focal length. On the other hand, the ideal tiptoe force F_{out} during P_1 explained in the previous section is characterized by exerting a leg contraction force before landing and becomes zero at touchdown. Taking into account these characteristics, the output is very similar to the sign-inverted desirable foot force F_{out} in Fig. 1.

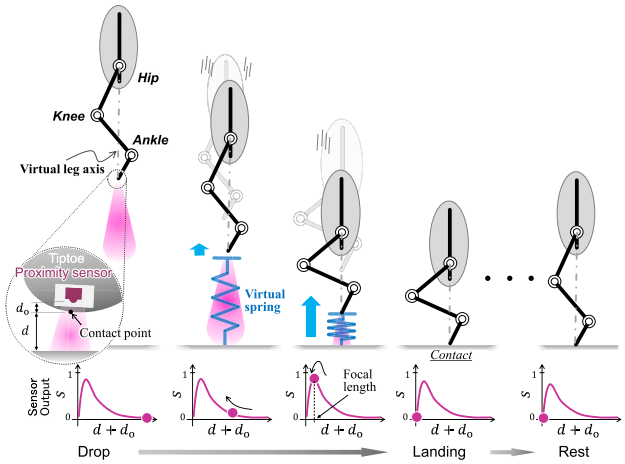

FIGURE 2. Basic idea of landing impact force mitigation control using proximity information of tiptoe.

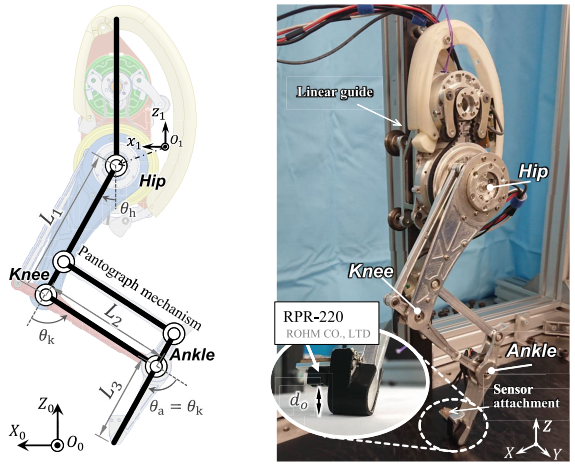

(a) Schematic (b) One-legged robot

FIGURE 3. One-legged robot with optical reflective sensor on tiptoe.

In general, to make the relationship between the output and distance unique, it is common to set d_o to a value greater than or equal to the focal length to ensure that only the sensor output above the focal length is used. In contrast, in our study, we focus on the similarity of the non-monotonicity between the ideal tiptoe force profile and the sensor output characteristics, including those below the focal length, and utilize the sensor output for pre-landing control of the robot.

C. PRE-LANDING CONTROL BASED ON PROXIMITY FEEDBACK

Figure 2 shows a conceptual diagram of the pre-landing control using the proximity sensor output. We realize the ideal change in toe force with a simple control law regarding the nonlinear output of the proximity sensor as the elastic force of a virtual spring. When the sensing surface and the ground are closest to each other in a tiptoe-contact state, the proximity sensor's output becomes very small, i.e., the elastic force of the virtual spring becomes small and does not affect the position controller.

In the rest of this section, we explain the proposed pre-landing control using a one-legged robot model. Figure 3(a) shows a schematic diagram of the one-legged robot used in the experiments. The robot is designed based on the skeletal structure of a hind limb of a small mammal and consists of hip, knee, and ankle joints. As shown in Fig. 3(b), a pantograph structure is used between the knee and ankle. Through this pantograph mechanism, the knee driving torque generated by the knee motor is transmitted to the ankle, and the ankle does not have its individual drive motor.

In the experiments, we constrained the robot's torso to vertical motion to consider only vertical movement of the robot in the sagittal plane in this paper to avoid complications. Thus, the following equation of motion of the robot is derived using the generalized coordinates $\boldsymbol{q} := [x, z, \phi, \boldsymbol{\theta}^\top]^\top$, where (x, z) represents the positions of CoG in the world frame, ϕ represents the pitch orientation angle of the torso and $\boldsymbol{\theta} := [\theta_h, \theta_k]^\top$ represents the hip and knee joint angles:

$$\boldsymbol{H}\ddot{\boldsymbol{q}} + \boldsymbol{D} + \boldsymbol{G} = \begin{bmatrix} \boldsymbol{0} \\ \boldsymbol{\tau} \end{bmatrix} + \begin{bmatrix} \boldsymbol{J}_l \\ \boldsymbol{J}_g \end{bmatrix}^\top \begin{bmatrix} f_l \\ \boldsymbol{f}_g \end{bmatrix}, \tag{1}$$

where $\boldsymbol{H}(\boldsymbol{q}) \in \mathbb{R}^{5\times5}$ is the inertia matrix, $\boldsymbol{D}(\boldsymbol{q}, \dot{\boldsymbol{q}}) \in \mathbb{R}^5$ is the nonlinear term including the centrifugal force, Coriolis force, and friction force, $\boldsymbol{G}(\boldsymbol{q}) \in \mathbb{R}^5$ is the gravity term, $\boldsymbol{\tau} \in \mathbb{R}^2$ is the driving torque vector, f_l is the horizontal reaction force applied to the robot's torso from the vertical linear guide, $\boldsymbol{f}_g = [f_x, f_z]^\top$ is the ground reaction force vector applied to the tiptoe, and $\boldsymbol{J}_l(\boldsymbol{q}) \in \mathbb{R}^{1\times5}$ and $\boldsymbol{J}_g(\boldsymbol{q}) \in \mathbb{R}^{2\times5}$ are the Jacobi matrices of the horizontal coordinates of the guide fixture and tiptoe coordinates with respect to the robot center of gravity, respectively. $\boldsymbol{f}_g = \boldsymbol{0}$ is satisfied when the robot is in the aerial phase.

Joint angle-based proportional-derivative (PD) control is a typical position control method for legged robots. The feedback torque $\boldsymbol{\tau}_{pd} \in \mathbb{R}^2$ by the PD controller is obtained as follows:

$$\boldsymbol{\tau}_{pd} = \boldsymbol{K}_p\left(\boldsymbol{\theta}_{des} - \boldsymbol{\theta}\right) - \boldsymbol{K}_d\dot{\boldsymbol{\theta}}, \tag{2}$$

where $\boldsymbol{\theta}_{des} \in \mathbb{R}^2$ is the desired joint angle vector, and $\boldsymbol{K}_p$ and $\boldsymbol{K}_d \in \mathbb{R}^{2\times2}$ are diagonal matrices with proportional and differential gains corresponding to the joint stiffness and viscosity, respectively. When $\boldsymbol{K}_p$ is large, the joint angle deviation due to disturbance can be small; however, a large toe reaction force is likely to be generated due to the displacement caused by landing. In contrast, when $\boldsymbol{K}_p$ is small, the leg compliance becomes high and the reaction force at landing may be reduced; however, the steady-state deviation of the joint angle tends to be large.

In this study, we apply the above explained proximity feedback control to the position PD-controlled legged robot. The proximity virtual force $\boldsymbol{F}_s$ corresponding to the magnitude of the sensor output s is provided as follows:

$$\boldsymbol{F}_s = -K_s s\boldsymbol{\eta}, \tag{3}$$

TABLE 1. Specifications for one-legged robot.

Robot parameters		
Parameter	Unit	Value
L_1	m	0.100
L_2	m	0.090
L_3	m	0.058
Total mass M	kg	0.505
Motor parameters		
Parameter	Unit	Value
Power	W	95
Peak torque	N m	0.4
Torque constant K_T	N m/A	0.0021
No-load speed	rpm	9000
Hip reduction ratio	-	3
Knee reduction ratio	-	4.5

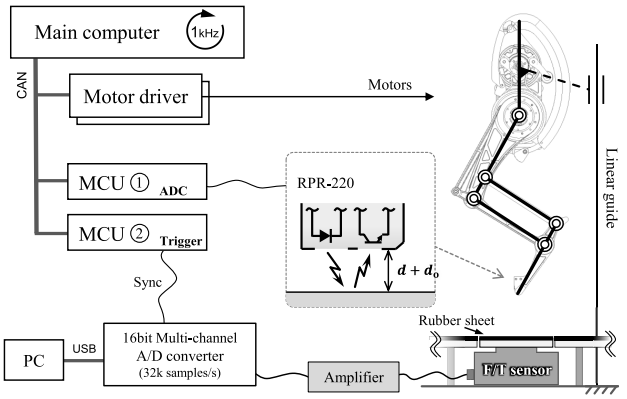

FIGURE 4. Controller and measurement system.

where K_s is the scale coefficient for the sensor output, and $\boldsymbol{\eta}$ is the unit normal vector of the detection surface. $\boldsymbol{F}_s$ is positive in the direction of leg extension. Equation (3) represents the elastic force due to a virtual spring with nonlinear characteristics between the tiptoe and the ground, as shown in Fig. 2. Thus, this force corresponds to a proximity virtual force that acts to contract the leg according to the distance between the tiptoe and the ground. Feedback torque is applied to each joint so that the robot acts as if the virtual force acts on the tiptoe.

The position of the tiptoe with respect to the coordinate system O_1 fixed on the hip of the robot body is calculated as

$$\begin{bmatrix} x_t \\ z_t \end{bmatrix} = \begin{bmatrix} (L_1 + L_3)\, S_h + L_2 S_{hk} \\ -(L_1 + L_3)\, C_h - L_2 C_{hk} \end{bmatrix}, \tag{4}$$

where $S_h = \sin\theta_h$, $S_{hk} = \sin(\theta_h - \theta_k)$, $C_h = \cos\theta_h$, and $C_{hk} = \cos(\theta_h - \theta_k)$. The Jacobi matrix of tiptoe $\boldsymbol{J}_h$ is obtained as

$$\boldsymbol{J}_h = \begin{bmatrix} (L_1 + L_3)\, C_h + L_2 C_{hk} & -L_2 C_{hk} \\ (L_1 + L_3)\, S_h + L_2 S_{hk} & -L_2 S_{hk} \end{bmatrix}. \tag{5}$$

Thus, the proximity feedback torque to each joint, $\boldsymbol{\tau}_s$, is calculated as follows:

$$\boldsymbol{\tau}_s = \boldsymbol{J}_h(\boldsymbol{\theta})^\top \boldsymbol{F}_s. \tag{6}$$

The sum of (2) and (6) is used as the system's control input torque $\boldsymbol{\tau}$.

$$\boldsymbol{\tau} = \boldsymbol{\tau}_{pd} + \boldsymbol{\tau}_s. \tag{7}$$

The scale coefficient of the sensor output K_s and the sensor offset distance d_o are design parameters that determine the characteristics of the proximity virtual force $\boldsymbol{F}_s$.

IV. ONE-LEGGED ROBOT WITH PROXIMITY SENSOR ON TIPTOE

The one-legged robot shown in Fig. 3(b) was developed to verify the feasibility of the proposed pre-landing control for landing impact mitigation. The specifications of the robot are listed in Table 1.

A permanent magnet synchronous motor, RoboDrive ILM38x06 (TQ-Systems GmbH), is used as the drive motor for the hip and knee joints of the robot leg. The drive torque for the hip is delivered from a motor mounted on the torso through timing belt-pulley transmission with a reduction ratio of 3. The knee motor is mounted on the same axis as the hip, which has a planetary gear reducer with a reduction ratio of 4.5, and transmitted to the knee joint axis through a parallel linkage mechanism. Reducers used on both drive joints have ultra-low reduction ratios and can be robust to impact forces due to low reflected inertia and low friction loss. This quasi-direct drive actuator configuration has high mechanical transparency and makes it possible to use good torque control capability by detecting motor current consumption [18]. The pantograph mechanism between the knee and ankle eliminates the need for an independent actuator for the ankle drive. Due to this structure, the legs can be lightweight, and most of the masses are concentrated at the root of the leg, resulting in a low-inertia robot leg. Most of the robot frames are made of duralumin, which is lightweight and strong.

An optical reflective sensor, RPR-220 (ROHM Co., Ltd.), a commercially available sensor packaged with infrared LEDs and photo-transistors, was adopted as a proximity sensor and introduced on the robot's tiptoe. The sensor is fixed to the foot link to face the ground in desired landing posture $\boldsymbol{\theta}_{des}$. The foot linkage surface around the sensor is covered with a black sheet to prevent multiple reflections. The sensor is attached to a sensor attachment, and the sensor offset distance d_o can easily be adjusted by changing the attachment.

The control system configuration and experimental system are illustrated in Fig. 4. Real-time control with a control frequency of 1 kHz was executed in a main computer. The output of the proximity sensor was measured with an AD converter (12-bit resolution) on the MCU mounted near the tiptoe. The mean value of five samples of the sensor output acquired in one control loop was sent to the main computer for feedback control. The target torque $\boldsymbol{\tau}_{ref}$ calculated based on the sensor output and the joint angle error was sent to each motor driver as a current command $\boldsymbol{I}_{ref}$ derived by $\boldsymbol{I}_{ref} = \boldsymbol{\tau}_{ref}/K_T$, where K_T is the torque constant and was controlled at a control frequency of 4 kHz in the driver. The rotation

TABLE 2. Experimental conditions.

Symbol	Unit	Value
$[K_\mathrm{p}\ K_\mathrm{d}]$	[Nm/deg Nm/(deg/s)]	(*high*) [0.12 0.0006], (*low*) [0.04 0.0002]
K_s	N	$0, 2, \ldots, 22, 24$
d_o	mm	$1, 3, 8$

angle, which is measured by the encoder (12-bit resolution) attached to the motor, and the motor current consumption were available from the driver. The main computer, motor driver, and power supply were located off-board.

V. LANDING EXPERIMENTS

Using the one-legged robot mentioned above, we performed landing experiments to verify the feasibility of the proposed pre-landing control based on tiptoe proximity information. To verify the pure effect of the proposed control on the vertical direction as the first step of this study, the motion of the robot torso was constrained only to vertical translation in the sagittal plane by a vertical linear guide, as illustrated in Fig. 4. In the experiments, the joint PD control of (2) was applied at a constant desired angle $\theta_{h,des} = 29\,\mathrm{deg}$ for the hip and $\theta_{k,des} = 86\,\mathrm{deg}$ for the knee. $\boldsymbol{\theta}_{des}$ was determined so that the virtual leg length axis was vertical in the desired posture. In this posture, the GRF produced for a vertically dropped robot acts in the almost vertical direction at the landing, and the robot is unlikely to reflect except in the vertical direction, making it easy to observe its landing behavior. We dropped the PD-controlled leg from a height where its tiptoe was 0.15 m above the landing surface. A force sensor (ATI-Gamma, ATI Industrial Automation) was installed under the landing surface, and an AD converter (16-bit resolution) of a DAQ system (USB-6221, National Instruments Corp.) was used to measure and record the GRF of the robot at 32 000 samples/s. The robot controller and GRF measurement system were synchronized using a synchronization signal. The GRF measured by the force sensor was only used for evaluation and not for robot control. A black 3-mm-thick rubber sheet was placed on the landing surface.

In the experiment, we analyzed the effects on the landing motion of the four parameters: the virtual stiffness and viscosity of robot joints $\boldsymbol{K}_p$ and $\boldsymbol{K}_d$, respectively, the scale coefficient of the proximity feedback K_s, and the offset distance between the toe contact point and the sensor detection surface d_o. The parameter ranges are summarized in Table 2.

In the experiments, we prepared two combinations of *high-gain mode* and *low-gain mode* for the joint PD control gain used for both the hip and knee. These values were determined so that the robot was not seriously damaged during landing. We prepared a total of 13 scale coefficients K_s for the sensor output in 2 N increments. $K_s = 0$ indicates no proximity feedback is applied. Three offset distances between the sensing surface and the contact point were used: $d_o = 8\,\mathrm{mm}$, which corresponds to the focal length of the sensor; $d_o = 3\,\mathrm{mm}$, which is the distance where the output at tiptoe contact is approximately half of the maximum output; and $d_o = 1\,\mathrm{mm}$, which is the minimum distance where the sensor package does not contact the ground at tiptoe contact.

With these different parameter combinations, we performed 10 experiments for each combination and recorded the proximity sensor output, joint angles, actuator current consumption, and vertical GRF. The behavior of the robot was recorded by a 600-fps high-speed camera.

VI. RESULTS AND DISCUSSIONS

A. EXPERIMENTAL RESULTS

A series of snapshots of the landing tiptoe under two different parameter combinations are shown in Fig. 5 as examples of the experiments. The time in the figure is adjusted so that the tiptoe contacts the ground at 0 s. In Fig. 5(a), the proximity feedback does not work because $K_s = 0$, which means that it shows a landing motion by a legged robot with only joint PD control applied. Figure 5(b) shows a landing motion by a legged robot with the proximity virtual force applied. From these snapshots, it can be seen that the proximity sensor feedback causes the leg to contract in advance just before landing. This contraction reduces the relative velocity between the tiptoe and the ground just before landing.

Several results of the landing experiments under different parameter combinations are shown in Figs. 6 and 7. Due to space limitations, we extracted the results necessary for a comparative analysis. These graphs show the proximity sensor output s, vertical GRF f_z, and joint angle errors $\Delta\theta = \theta_{des} - \theta$ for 0.35 seconds before and after contact. We regarded the rise of the GRF f_z as the touchdown time and set it to $t_c = 0$. The solid line in the graph shows the mean value and the colored area shows the max-min range of the 10 trials. Figures 6 a-1, b-1, and c-1 show the results of the *high-gain mode*, while a-2, b-2, and c-2 show the results of the *low-gain mode*. The differences in results due to PD controller gain values are particularly evident in the GRF profile and the joint angle displacement in P_2. Figure 7 shows the results under the *high-gain mode* for different K_s and d_o. Comparing the sensor output s, a difference can be observed just before landing depending on the offset distance d_o. In addition, there is a difference in the magnitude of s after landing in different d_o. The knee joint flexed due to the GRF in all experiments, while the angular displacement and flexion speed differed depending on the conditions.

We use the following four evaluation values in this paper: the landing initial peak impact force F_I; the maximum vertical GRF F_{max}; vertical velocity of tiptoe at the moment of landing v_c; and the time when tiptoe force F_{out} to be zero or greater ΔT_X. v_c is calculated by the following equation, assuming that the inertia of the leg is small and does not affect the motion of the robot's CoG:

$$v_c = -\left(2\,g\left(h_{ini} + \Delta z_{t,c}\right)\right)^{\frac{1}{2}} + \dot{z}_{t,c}, \tag{8}$$

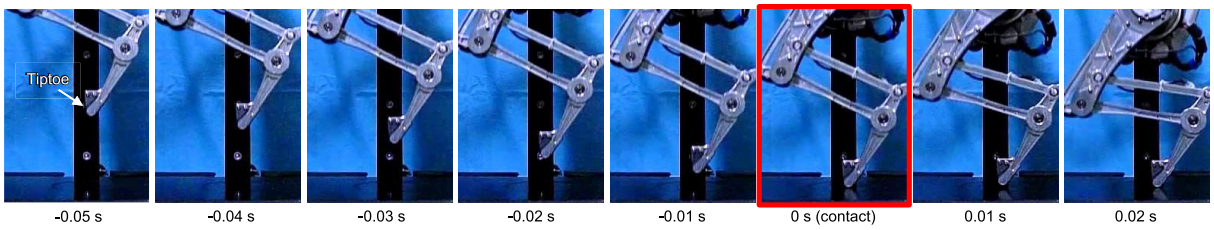

(a) *low-gain mode*, $K_s = 0\,\mathrm{N}$, $d_o = 1\,\mathrm{mm}$

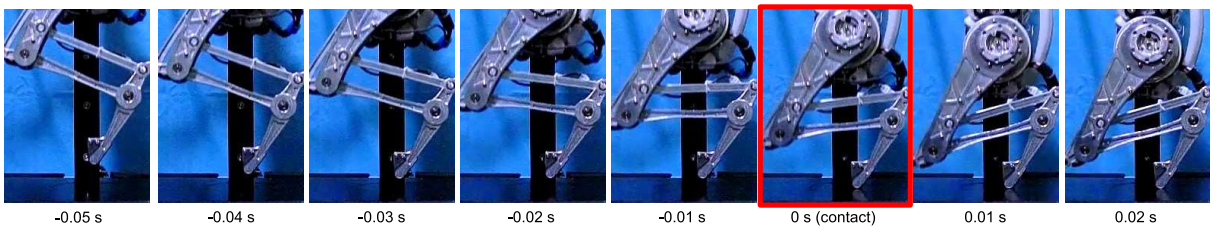

(b) *low-gain mode*, $K_s = 12\,\mathrm{N}$, $d_o = 1\,\mathrm{mm}$

FIGURE 5. **Snapshots of landing experiments.**

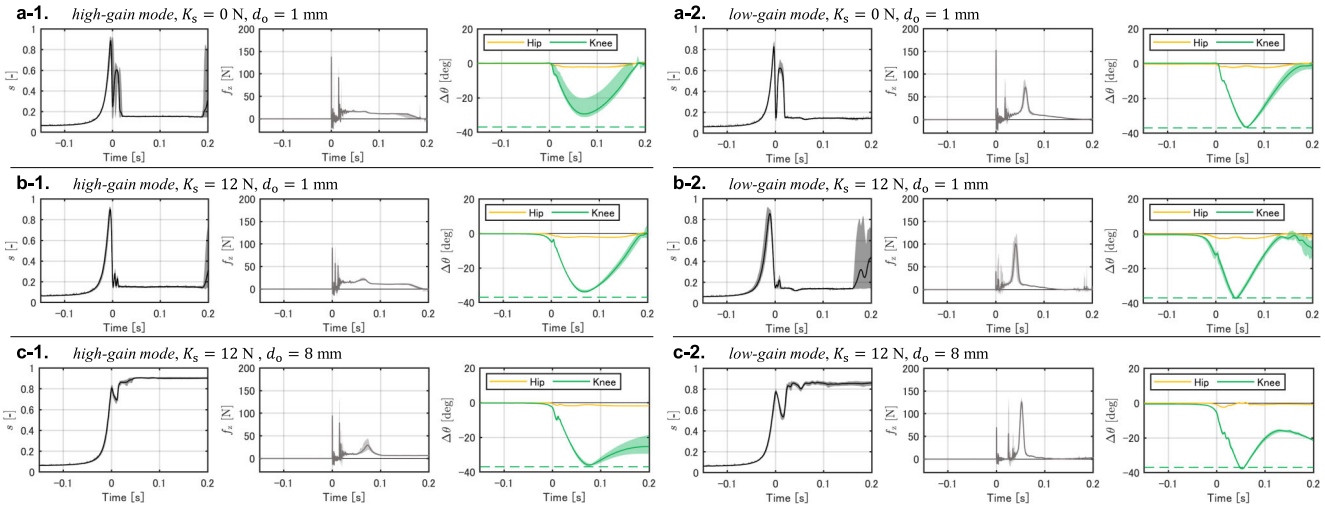

FIGURE 6. **Comparison between results in *high-gain mode* and *low-gain mode*.**

where g is the gravitational acceleration, h_{ini} is the initial tiptoe height (0.15 m), $\Delta z_{t,c} = z_{t,c} - z_{t,des}$ is the error of the actual vertical tiptoe position ($z_{t,c}$) from the desired position ($z_{t,des}$) in the landing position, and $\dot{z}_{t,c}$ is the vertical tiptoe velocity in the O_1 coordinate system at the moment of ground contact as obtained by the time differentiation of (4). v_c corresponds to $\dot{d}(t_c)$ in Fig. 1. The tiptoe output force in the direction of the leg length axis is obtained as follows:

$$F_{out} = F_{pd} + F_v \tag{9}$$

$$= \boldsymbol{\tau}^\top \boldsymbol{J}_h^{-1} \boldsymbol{\eta}, \tag{10}$$

where F_{pd} and F_v are tiptoe output forces on the leg length axis due to the joint PD control torque $\boldsymbol{\tau}_{pd}$ and the proximity sensor feedback torque $\boldsymbol{\tau}_s$, respectively. F_{out}, F_{pd}, and F_v are positive in the direction of leg extension. From (3), $F_v < 0$ is satisfied if $K_s \neq 0$ under $s > 0$. ΔT_X is defined as the elapsed time from the landing to the positive F_{out} generated; i.e., F_{pd} exceeds $-F_v$ due to the large angular displacement. ΔT_X can be negative if $F_{pd} > -F_v$ is satisfied before landing; e.g., when d_o is shorter than the focal length, the sensor output s suddenly decreases when the tiptoe comes closest to the ground, and thus $-F_v$ drops below F_{pd}.

Figure 8 summarizes the four evaluation values explained above as obtained using the experimental result in each parameter combination. The error bars in the graphs indicate the max-min range for 10 trials. Regardless of the joint PD control gain magnitude, the closer the tiptoe velocity v_c is to 0, the smaller F_I is. Under the *high-gain mode*, the landing impact force F_I decreases monotonically as K_s increases, independent of the proximity sensor offset distance d_o. Under the *low-gain mode*, F_I meets its minimum value when

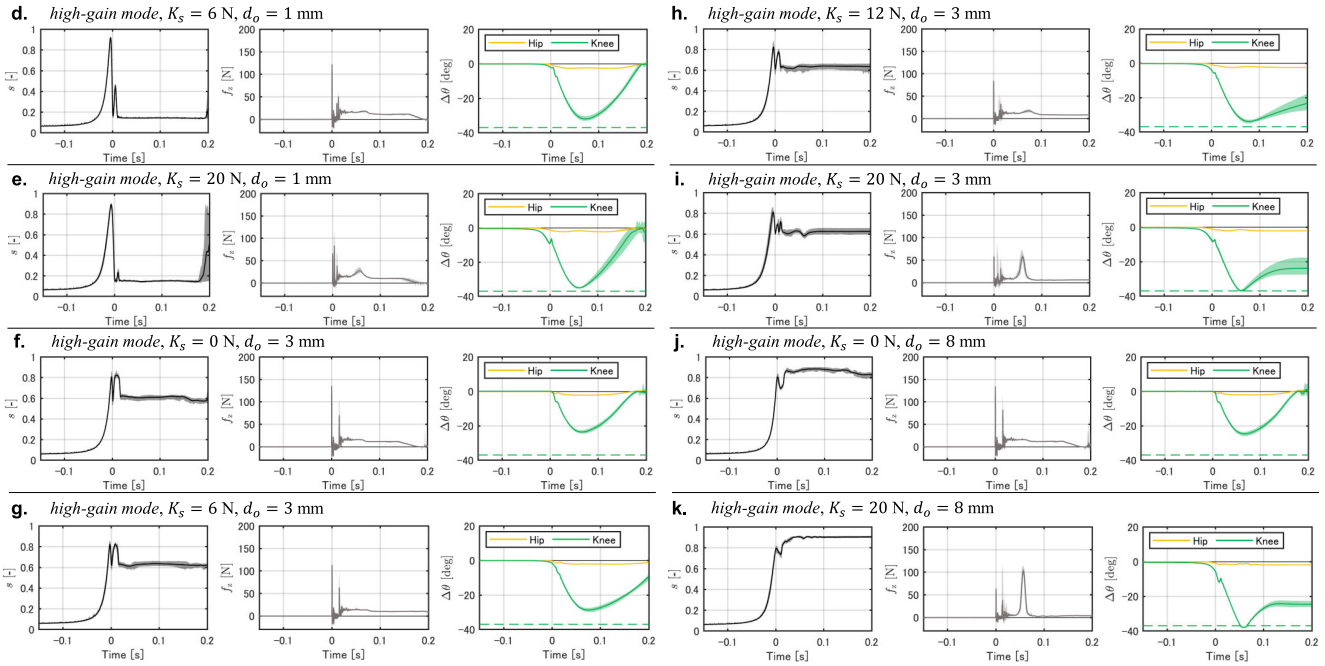

FIGURE 7. Comparison between results with different K_S and d_o.

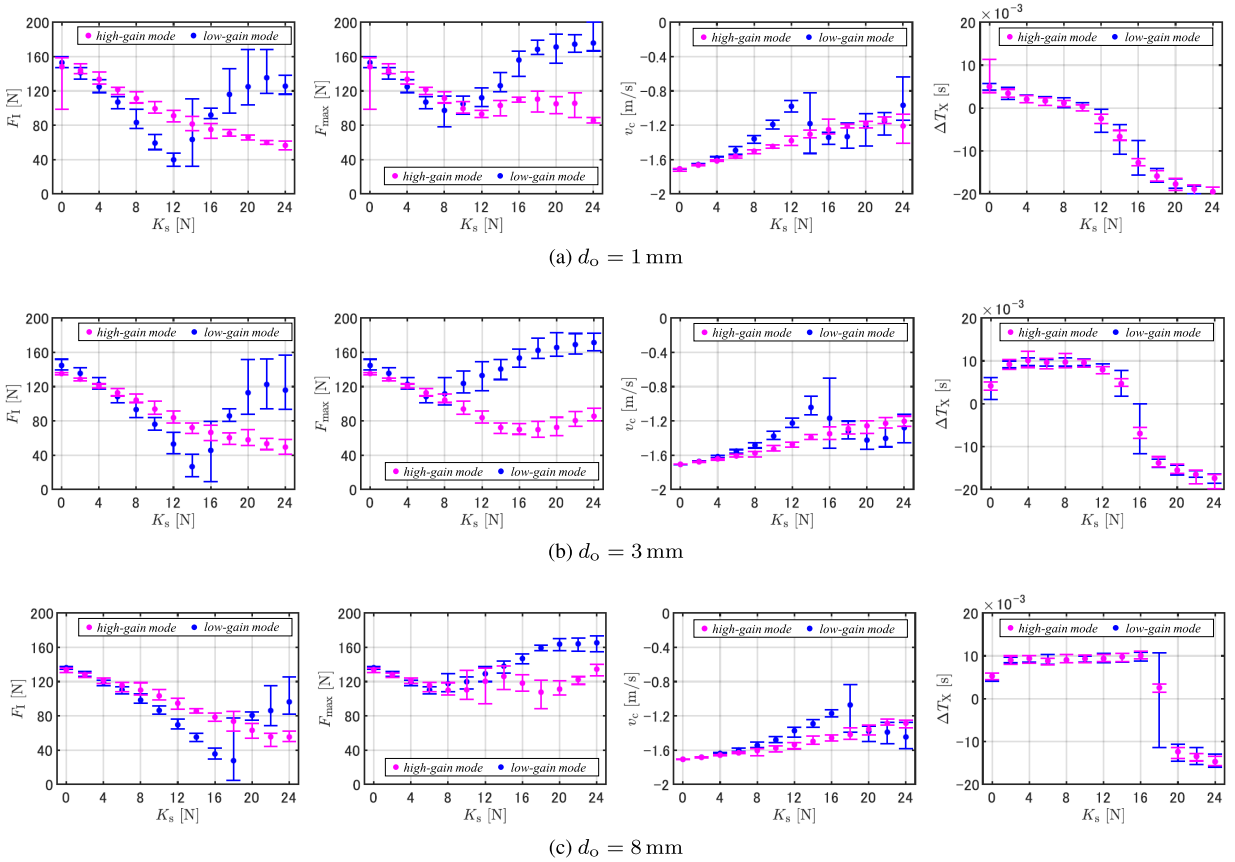

FIGURE 8. Results of landing experiment.

TABLE 3. Evaluation of best result.

Condition	F_{I} (N)	$F_{\max}$ (N)	$\Delta z_{\mathrm{t,e}}$ (m)
BEST			
high-gain mode $K_{\mathrm{s}} = 24\,\mathrm{N}$ $d_{\mathrm{o}} = 1\,\mathrm{mm}$	56.47	85.54	-0.015
Baseline			
high-gain mode $K_{\mathrm{s}} = 0\,\mathrm{N}$ $d_{\mathrm{o}} = 8\,\mathrm{mm}$	133.7	133.7	-0.0052

$K_s = 12\,\mathrm{N}$ for $d_o = 1\,\mathrm{mm}$, $K_s = 14\,\mathrm{N}$ for $d_o = 3\,\mathrm{mm}$, and $K_s = 18\,\mathrm{N}$ for $d_o = 8\,\mathrm{mm}$. Furthermore, ΔT_X is close to 0 at K_I, where F_I takes the minimum value. In other words, the minimum contact force is obtained when the ground contact occurs in $F_{out} = 0$ due to the leg extension force by the joint PD controller and the leg contraction force by the proximity virtual force being in opposition. The maximum GRF, F_{max}, tends to be approximately the same or lower under the *high-gain mode* than under the *low-gain mode*. Under the *low-gain mode*, F_{max} takes a minimum value at a relatively small value of $K_s = 6$ or 8 and tends to increase at larger K_s.

B. DISCUSSIONS

Given the ideal landing requirements described in Section III, we evaluate the landing test results from the following evaluation items:

1) The magnitude of the impact force at touchdown: F_I.
2) Maximum vertical GRF after landing: F_{max}.
3) Posture error in equilibrium posture: $|\Delta z_{t,e}|$.

We adopted $t_e = 0.45\,\mathrm{s}$ as the time when the landing motion was complete and the robot rested at equilibrium posture. $\Delta z_{t,e}$ is obtained from $\boldsymbol{\theta}_{des}$ and $\boldsymbol{\theta}$ at $t = t_e$ using (4) and represents the hip height error. We define an evaluation index ϵ that comprehensively evaluates them as follows:

$$\epsilon = \frac{E(F_I) + E(F_{max}) + E(|\Delta z_{t,e}|)}{3}, \tag{11}$$

where function E is defined as follows:

$$E(\alpha) = \frac{\alpha - \min(\alpha)}{\max(\alpha) - \min(\alpha)}. \tag{12}$$

Equation (11) represents the sum of each evaluation item that is normalized in the measured range ($0 \leq E \leq 1$). Consequently, $0 \leq \epsilon \leq 1$ holds. This means that a landing motion with a smaller ϵ is closer to the ideal landing motion.

ϵ in all combinations is summarized in Fig. 9. The smallest ϵ was obtained under *high-gain mode*, $K_s = 24\,\mathrm{N}$, and $d_o = 1\,\mathrm{mm}$ (hereafter called "BEST"). Here, we determine the landing result under *high-gain mode*, $K_s = 0\,\mathrm{N}$, $d_o = 8\,\mathrm{mm}$ (shown in Fig. 7 j), in which the proximity sensor feedback was not used, as a baseline. The evaluation indices obtained by BEST and baseline are listed in Table 3. Compared to the result of the baseline, the impact force F_I just after ground contact by BEST was reduced to 42 %, and the maximum vertical GRF F_{max} was reduced to 64 %. $|\Delta z_{t,e}|$ increased by 0.01 m, but this is negligibly small compared to the leg length in the desired posture ($z_{t,des} = 0.186\,\mathrm{m}$). From the above results, it can be concluded that the proposed pre-landing control based on the proximity information on tiptoes is effective for landing legged robots.

Next, we discuss the effect of each parameter on the landing motion.

1) JOINT PD CONTROLLER GAINS K_p AND K_d

From Fig. 9, it can be seen that ϵ under the *high-gain mode* is equal to or smaller than that under the *low-gain mode* in most cases. As shown in Fig. 6, because the joint stiffness is high under the *high-gain mode*, the impact force at the ground contact is inevitably greater. Under the *low-gain mode*, the landing impact F_I is minimized when $\Delta T_X \approx 0$, as shown in Fig. 8, which is in accordance with the hypothesis of landing impact mitigation explained in Section III. On the other hand, the GRF after landing tends to be larger under the *low-gain mode*. The maximum value of GRF F_{max} is larger under the *low-gain mode* in most case, and the difference is significant for larger K_s values. The graph of joint angular displacement $\Delta\theta$ in Fig. 6 shows that the knee angle reached the flexion limit under the *low-gain mode*. This indicates that the leg contraction due to the fall of the torso after touchdown could not be sufficiently decelerated because of the low joint stiffness and damping, the upper and lower links around the knee collided with each other at the flexion limit, and this collision caused a large F_{max}. In the case of a legged robot landing where the load changes immediately before and after landing, achieving the desired low-impulse landing only by joint compliance control with a constant gain is challenging.

2) PROXIMITY VIRTUAL FORCE COEFFICIENT K_s

As shown in Fig. 9, the change tendency of ϵ is similar under all conditions when $K_s \leq 8\,\mathrm{N}$, but the tendency differs depending on the condition in large K_s. For example, from Figs. 7 f, g, h, and i (with $d_o = 3\,\mathrm{mm}$), it can be seen that F_I can be reduced by introducing proximity feedback compared to that when $K_s = 0$, which is without proximity feedback. The larger K_s involves the larger virtual force F_v, which increases in response to the proximity sensor output s, and the leg contraction in the pre-landing motion becomes larger. As shown in Fig. 8, the relative velocity between the tiptoe and the ground v_c can be brought close to zero, as explained in Section III, resulting in landing impact mitigation. The leg contraction prior to touchdown also has the advantage of securing sufficient clearance between the tiptoe and the ground just before touchdown, which allows for a longer control time before landing. However, note that if K_s is too large, then the leg contracts too much before landing, and the fall speed of the torso after landing could not sufficiently be decelerated. In the case of $d_o = 3, 8\,\mathrm{mm}$, where the sensor output s is medium or high even in the tiptoe-contact state after landing, $|\Delta z_{t,e}|$ is large because it involves a large joint

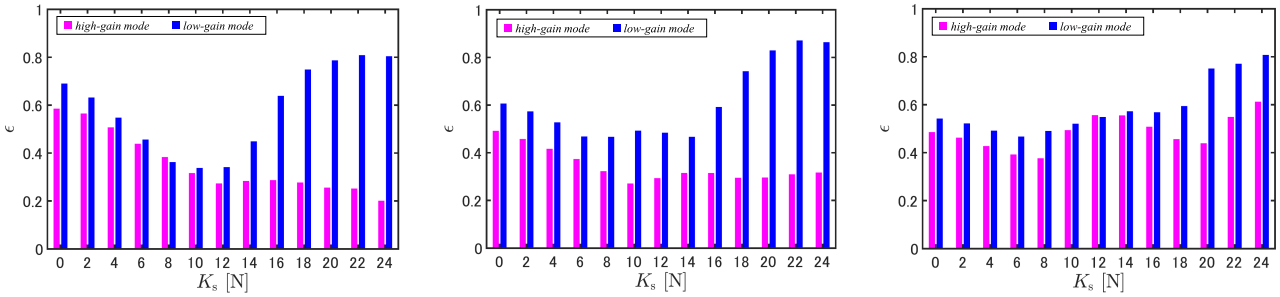

(a) $d_o = 1$ mm (b) $d_o = 3$ mm (c) $d_o = 8$ mm

FIGURE 9. Evaluation of landing performance.

angular displacement and fluctuation to obtain F_{out} that is balanced by the body weight (Figs. 8(b) and (c)).

3) OFFSET DISTANCE d_o

As shown in Fig. 9, ϵ is relatively high for any K_s with $d_o = 8$ mm. The magnitude of the landing impact force F_I is not significantly affected by d_o values. In the case where the offset distance is equal to the focal length, $d_o = 8$ mm, the sensor output s is maximized in the tiptoe-contact state, and a large virtual force F_v always acts on the tiptoe. The large F_v made F_{out} smaller while standing, and there was not sufficient force to support its own weight. As a result, the large steady deviation $|\Delta z_{t,e}|$ causes a large ϵ. For the same reason, ϵ does not decrease when $K_s \geq 10$ N with $d_o = 3$ mm. In contrast, when $d_o = 1$ mm, the robot was able to reach an equilibrium posture close to the desired posture after landing because the sensor output s in the tiptoe-contact state was sufficiently small. This result indicates that using our proposed control, it is not necessary to switch the joint angle-based position control before and after landing.

Thus, a proximity sensor that can acquire proximity information before touchdown and has an output characteristic where the output is small in the tiptoe-contact state is suitable for legged robot pre-landing control. This conclusion is consistent with the assumptions in Section III, and we achieved landing impact mitigation and posture deviation reduction without switching between landing control and position control before and after landing using pre-landing control based on optical reflective sensor feedback. By introducing a proximity sensor on a tiptoe that comes into contact with the environment, the relative relationship between them can be obtained directly and is not affected by occlusion or modeling errors. In other words, feedback control is not affected by any sensor errors or sampling rates used for pose estimation and can be performed using only local information. The quick and precise local relative state sensing ability of the proximity sensor is effective for the challenging problem of landing impact mitigation. The proposed method has the potential to reflexively adapt to sloping ground, unexpected disturbances and the ground environmental changes before colliding. On the other hand, when landing on the ground with low light reflectance or in an environment where strong sunlight shines, the current prototype system may misrecognize the ground and eventually fail to land. These can be improved by designing a tiptoe proximity sensor available for the practical usage environment of a legged robot.

VII. CONCLUSION

We proposed a pre-landing control method based on tiptoe proximity information for a legged robot. The proposed control utilizes the non-monotonic proximity sensor output and feeds it back as a proximity virtual force on tiptoe. The control framework can be easily integrated into the existing motion control because it does not affect the robot motion control during the tiptoe-contact state. Through drop experiments from a certain height with the robot applying the proposed pre-landing control, it is shown that the landing impact force can be mitigated. This approach can be expected to be effective even when used in a legged robot with more than a dozen joints because the proposed control method is only based on the relative information with the ground without involving occlusion and modeling error. The proposed method is also effective for dynamic movements such as landing after jumping from/to a high place due to the high-speed response of the proximity sensor.

In future work, we will design a tiptoe proximity sensor that can be used in various ground conditions and environments where a legged robot is practically used. Moreover, we will design control parameters to negotiate conditions where the approach speed and acceleration at landing are different. Then, we will apply this control scheme to a dynamic-legged robot that we are currently developing and perform some experiments, including a series of dynamic motions from high jumps to quiet landings.

REFERENCES

[1] *Boston Dynamics. Spot*. Accessed: Sep. 15, 2021. [Online]. Available: https://www.bostondynamics.com/spot

[2] G. Bledt, M. J. Powell, B. Katz, J. Di Carlo, P. M. Wensing, and S. Kim, "MIT cheetah 3: Design and control of a robust, dynamic quadruped robot," in *Proc. IEEE/RSJ Int. Conf. Intell. Robots Syst. (IROS)*, Oct. 2018, pp. 2245–2251.

[3] M. Hutter, C. Gehring, D. Jud, A. Lauber, C. D. Bellicoso, V. Tsounis, J. Hwangbo, K. Bodie, P. Fankhauser, M. Bloesch, R. Diethelm, S. Bachmann, A. Melzer, and M. Hoepflinger, "ANYmal—A highly mobile and dynamic quadrupedal robot," in *Proc. IEEE/RSJ Int. Conf. Intell. Robots Syst. (IROS)*, Oct. 2016, pp. 38–44.

[4] *Agility Robotics*. Digital Accessed: Sep. 15, 2021. [Online]. Available: https://www.agilityrobotics.com/#cover
[5] J. J. Rond, M. C. Cardani, M. I. Campbell, and J. W. Hurst, "Mitigating peak impact forces by customizing the passive foot dynamics of legged robots," *J. Mech. Robot.*, vol. 12, no. 5, Oct. 2020, Art. no. 051010.
[6] R. M. Alexander, "Three uses for springs in legged locomotion," *Int. J. Robot. Res.*, vol. 9, no. 2, pp. 53–61, 1990.
[7] J. Cho and K. Kong, "The analysis of mechanical structure of a robotic leg in running for impact mitigation," *Appl. Sci.*, vol. 10, no. 4, p. 1365, Feb. 2020.
[8] J. Chen, Z. Liang, Y. Zhu, C. Liu, L. Zhang, L. Hao, and J. Zhao, "Towards the exploitation of physical compliance in segmented and electrically actuated robotic legs: A review focused on elastic mechanisms," *Sensors*, vol. 19, no. 24, p. 5351, Dec. 2019.
[9] F. Iida, J. Rummel, and A. Seyfarth, "Bipedal walking and running with spring-like biarticular muscles," *J. Biomech.*, vol. 41, no. 3, pp. 656–667, 2008.
[10] A. Spröwitz, A. Tuleu, M. Vespignani, M. Ajallooeian, E. Badri, and A. J. Ijspeert, "Towards dynamic trot gait locomotion: Design, control, and experiments with cheetah-cub, a compliant quadruped robot," *Int. J. Robot. Res.*, vol. 32, no. 8, pp. 932–950, Jul. 2013.
[11] R. Sato, I. Miyamoto, K. Sato, A. Ming, and M. Shimojo, "Development of robot legs inspired by bi-articular muscle-tendon complex of cats," in *Proc. IEEE/RSJ Int. Conf. Intell. Robots Syst. (IROS)*, Sep. 2015, pp. 1552–1557.
[12] J. H. Park, "Impedance control for biped robot locomotion," *IEEE Trans. Robot. Autom.*, vol. 17, no. 6, pp. 870–882, Dec. 2001.
[13] C. Semini, V. Barasuol, T. Boaventura, M. Frigerio, M. Focchi, D. G. Caldwell, and J. Buchli, "Towards versatile legged robots through active impedance control," *Int. J. Robot. Res.*, vol. 34, no. 7, pp. 1003–1020, Jul. 2015.
[14] J. Jo and Y. Oh, "Impedance control of humanoid walking on uneven terrain with centroidal momentum dynamics using quadratic programming," in *Proc. IEEE/RSJ Int. Conf. Intell. Robots Syst. (IROS)*, Oct. 2020, pp. 3525–3530.
[15] X. Yu, W. He, Q. Li, Y. Li, and B. Li, "Human-robot co-carrying using visual and force sensing," *IEEE Trans. Ind. Electron.*, vol. 68, no. 9, pp. 8657–8666, Sep. 2021.
[16] M. Hutter, C. Gehring, M. Bloesch, M. A. Hoepflinger, C. D. Remy, and R. Siegwart, "StarlETH: A compliant quadrupedal robot for fast, efficient, and versatile locomotion," in *Proc. Int. Conf. Climbing Walking Robots*, Jul. 2012, pp. 483–490.
[17] Y. H. Lee, Y. H. Lee, H. Lee, L. T. Phan, H. Kang, Y. B. Kim, and H. R. Choi, "Development of torque controllable leg for running robot, AiDIN-IV," in *Proc. IEEE/RSJ Int. Conf. Intell. Robots Syst. (IROS)*, Sep. 2017, pp. 4125–4130.
[18] P. M. Wensing, A. Wang, S. Seok, D. Otten, J. Lang, and S. Kim, "Proprioceptive actuator design in the MIT cheetah: Impact mitigation and high-bandwidth physical interaction for dynamic legged robots," *IEEE Trans. Robot.*, vol. 33, no. 3, pp. 509–522, Jun. 2017.
[19] S. Kalouche, "GOAT: A legged robot with 3D agility and virtual compliance," in *Proc. IEEE/RSJ Int. Conf. Intell. Robots Syst. (IROS)*, Sep. 2017, pp. 4110–4117.
[20] B. Katz, J. D. Carlo, and S. Kim, "Mini cheetah: A platform for pushing the limits of dynamic quadruped control," in *Proc. Int. Conf. Robot. Autom. (ICRA)*, May 2019, pp. 6295–6301.
[21] F. Grimminger, A. Meduri, M. Khadiv, J. Viereck, M. Wuthrich, M. Naveau, V. Berenz, S. Heim, F. Widmaier, T. Flayols, J. Fiene, A. Badri-Sprowitz, and L. Righetti, "An open torque-controlled modular robot architecture for legged locomotion research," *IEEE Robot. Autom. Lett.*, vol. 5, no. 2, pp. 3650–3657, Apr. 2020.
[22] Y. Sakakibara, K. Kan, Y. Hosoda, M. Hattori, and M. Fujie, "Low-impact foot trajectory for a quadruped walking machine," *Adv. Robot.*, vol. 7, no. 4, pp. 343–360, Jan. 1992.
[23] E. Ohashi and K. Ohnishi, "Variable compliance control based on soft-landing trajectory for hopping robot," in *Proc. 30th Annu. Conf. IEEE Ind. Electron. Soc.*, vol. 1. Busan, South Korea, Nov. 2004, pp. 117–122.
[24] S. Sakka, N. Sian, and K. Yokoi, "Motion pattern for the landing phase of a vertical jump for humanoid robots," in *Proc. IEEE/RSJ Int. Conf. Intell. Robots Syst.*, Oct. 2006, pp. 5477–5483.
[25] C. Dong, X. Chen, Z. Yu, Z. Huang, Q. Li, Q. Zhou, and Q. Huang, "A novel hierarchical control strategy for biped robot walking on uneven terrain," in *Proc. IEEE-RAS 19th Int. Conf. Humanoid Robots (Humanoids)*, Oct. 2019, pp. 140–145.
[26] S. E. Navarro, S. Muhlbacher-Karrer, H. Alagi, H. Zangl, K. Koyama, B. Hein, C. Duriez, and J. R. Smith, "Proximity perception in human-centered robotics: A survey on sensing systems and applications," *IEEE Trans. Robot.*, early access, Nov. 1, 2022, doi: 10.1109/TRO.2021.3111786.
[27] D. Hughes, J. Lammie, and N. Correll, "A robotic skin for collision avoidance and affective touch recognition," *IEEE Robot. Automat. Lett.*, vol. 3, no. 3, pp. 1386–1393, Jul. 2018.
[28] Y. Ding and U. Thomas, "Collision avoidance with proximity servoing for redundant serial robot manipulators," in *Proc. IEEE Int. Conf. Robot. Autom. (ICRA)*, May 2020, pp. 10249–10255.
[29] Y. Hirai, Y. Suzuki, T. Tsuji, and T. Watanabe, "High-speed and intelligent pre-grasp motion by a robotic hand equipped with hierarchical proximity sensors," in *Proc. IEEE/RSJ Int. Conf. Intell. Robots Syst. (IROS)*, Oct. 2018, pp. 7424–7431.
[30] K. Koyama, M. Shimojo, A. Ming, and M. Ishikawa, "Integrated control of a multiple-degree-of-freedom hand and arm using a reactive architecture based on high-speed proximity sensing," *Int. J. Robot. Res.*, vol. 38, no. 14, pp. 1717–1750, Dec. 2019.
[31] H. Arita and Y. Suzuki, "Contact transition control by adjusting emitting energy of proximity sensor," *Adv. Robot.*, vol. 35, no. 2, pp. 93–107, Jan. 2021.
[32] J. R. Guadarrama-Olvera, F. Bergner, E. Dean, and G. Cheng, "Enhancing biped locomotion on unknown terrain using tactile feedback," in *Proc. IEEE-RAS 18th Int. Conf. Humanoid Robots (Humanoids)*, Nov. 2018, pp. 1–9.

RYUKI SATO (Member, IEEE) received the B.E., M.E., and Ph.D. degrees in engineering from The University of Electro-Communications (UEC), Tokyo, Japan, in 2014, 2016, and 2020, respectively. He was a Japan Society for the Promotion of Science (JSPS) Research Fellow, from 2017 to 2019. He is currently a designated Assistant Professor with the Department of Aerospace Engineering, Graduate School of Engineering, Nagoya University, Aichi, Japan. His research interests include bio-inspired robotics, design, and control of legged robots, and dynamic legged locomotion.

HIKARU ARITA (Member, IEEE) received the B.E., M.E., and Ph.D. degrees from The University of Electro-Communications (UEC), Tokyo, Japan, in 2012, 2014, and 2019, respectively. From 2014 to 2016, he worked at OMRON Corporation. Since 2019, he has been an Assistant Professor with Ritsumeikan University. His research interests include proximity sensor and sensor-based control.

AIGUO MING (Member, IEEE) received the Ph.D. degree in precision machinery engineering from The University of Tokyo, Tokyo, Japan, in 1990. He is currently a Professor with the Department of Mechanical Engineering and Intelligent Systems, The University of Electro-Communications, Tokyo. His current research interests include biomimetic hyper-dynamic robotics, soft robotics, intelligent robot hands, and precise measuring systems.